Research Article Vol. 13, No. 1 / 1 Jan 2023 / Optical Materials Express 130
Optical Materials EXPRESS

Fabrication of a large scale metasurface with high resolution and enhanced absorption

Muath Al Hasan,[1] Zaka Ullah,[1,*] Illani Nawi,[2] and Ismail Ben Mabrouk[3]

[1] *College of Engineering, Al Ain University, 64141, United Arab Emirates*
[2] *Department of Electrical and Electronic Engineering, Universiti Teknologi PETRONAS, Perak 32610, Malaysia*
[3] *Department of Electrical Engineering, Durham University, Durham, UK*
[*] *zakaullah.zaibullah@aau.ac.ae*

Abstract: Plasmonic metasurface nanostructures have the potential to enable nonlinear optical functionality in metasurfaces by reducing power operating thresholds and enabling ultra-thin subwavelength devices. However, low absorption caused by resistive losses of unwanted metallic appearance and irregular corners in the fabrication process significantly reduces this promise, leading the metasurface community toward the new approaches to fabricate large area metasurfaces with Electron Beam lithography (EBL). In this article, with controlled proximity effect and high dose exposure rate in EBL setup, large area (2 cm^2) metasurfaces are fabricated with high resolution of structure. The effect of absorption resonance in Infrared (LWIR) is experimentally studied through Fourier Transform Infrared Spectroscopy (FTIR). The results signify that the metasurface with high resolution and fine metallic corners outperforms the fabricated prototype with metal residue and non-uniform corners. When compared to conventional EBL, our nanofabrication approach speeds the patterning time by three times. The experimental measurements reveal enhanced absorption performance at 8 µm wavelength. Whereas, the developed metasurface is numerically studied to explain the absorption performance with plasmonic field distributions. This approach could be used in optoelectronic devices involving plasmonic applications, such as biosensing and infrared imaging.

1. Introduction

Strong field coupling between plasmonic metasurface nanostructures has been proven and facilitated by squeezing photons into deep sub-wavelength volumes and a few nanometer gaps [1]. Plasmonic metasurface structures have been reported to acquire massive field enhancements in a small volume, referred to as localized field area. The strength and location of localized plasmon fields are determined by the metasurface design [2], size [3], and dielectric media [4]. Electric fields can be greatly amplified in the close vicinity of sharp metal edges or sub-nanometer size gaps, as per antenna theory [5]. Light interactions with plasmonic metasurface structures become more prominent when the feature size or gap size of the structure reduces. A conventional platform (specifically square or triangular plasmonic designs) has been established in this context to confine the light into a very small volume [6], on which more complicated geometric structures are built. The reduction in the size of metallic structures enables enhanced electromagnetic (EM) fields into localized confine fields at deep sub-wavelength volumes, allowing for exciting applications such as quantum plasmonic [7], bio-sensing [8], and imaging [9].

The development of novel approaches and techniques for the fabrication of nanoscale plasmonic structures with a spatial resolution of tens of microns is required to keep nanotechnology and optoelectronic industries growth [10]. Direct-write lithography also known as electron beam lithography (EBL), which uses an electron beam to interact with a polymer resist, is one of the most advanced and in-demand technologies [11]. Although, EBL has high throughput in

#469973 https://doi.org/10.1364/OME.469973
Journal © 2023 Received 7 Jul 2022; revised 8 Sep 2022; accepted 13 Sep 2022; published 13 Dec 2022

fabricating plasmonic structures but hinders the reliability to develop large arrays of metasurfaces with sharp corners and edges [12]. The sharp corners are the crucial element for the localized plasmon fields propagating along the metasurface geometry [13]. There are several challenges posed by EBL setup when it comes to fabricating a large array of metasurfaces having sharp metal tips and corners. The main disadvantage of EBL is the exposure speed (about 10^7 pixels per second) and the cost of mass production [14]. Whereas, the chemical characteristics of polymers are affected by high-dose electron irradiation, resulting in hardening or overexposure [15]. Furthermore, the electron beam proximity effect occurs when a specific area is exposed to an E-beam, and the nearby area to the incident E-beam receives undesired irradiation as well [16]. Different approaches are being used to fabricate sharper and narrower-gap metallic metasurfaces for higher field enhancements, including but not limited to EBL.

In literature [17], the single-spot EBL technique is demonstrated with controllable geometric parameters to cater the overexposure limitation, thus enabling the fabrication rate ten times faster as compared to conventional lithography. The method of nanostencil lithography [7] is utilized for high throughput of large area nanorod antenna arrays by preparing nanostencil with a low electron dose of EBL. In Ref. [18], the two-photon polymerization method is employed to achieve sharp metal tips of the plasmonic diatomic metasurface. The proximity effect correction in EBL [19] is studied for fabricating uniform corners of metasurfaces with a control exposure rate for enhancing efficiency. The concept of cascaded domino lithography is experimentally validated for constructing sharp tips bowtie antennas with a "fall-to-raise" scheme [20]. In another study [9], L shaped uniform metasurface array is realized with glanced angle techniques through nanoimprint lithography for optical chirality.

In this article, we demonstrated large area metasurface fabrication with the EBL technique to realize uniform corners in hexagons and cross shape metasurfaces. The method is based on controlling the proximity effect and correct exposure dose to define fine patterns on Poly methyl methacrylate (PMMA) resist, resulting in high resolution and quality metasurface prototypes. The characterization results indicate that metasurfaces with uniform metal corners attain higher field enhancement with strong absorption at long wavelength infrared regions (LWIR). The article is divided into the following sections, with section 2 studying the simulation and fabrication theory utilizing Monte Carlo simulations. Section 3 examines the metasurface prototyping using our suggested EBL approach and conventional method. Section 4 discusses the optical and structural characterization methods for the developed metasurface. Section 5 presents the result and analysis of the findings, and Section 6 draws the conclusion.

2. Monte Carlo simulations and theory for fabrication process

In this section, a theoretical study is conducted for the fabrication process using Monte Carlo simulation tools (CASINO and EBL simulator) to understand the backscattering trajectories resulting from the proximity effect and their effect on the profile of the developed pattern. The fabrication of metasurface under normal conditions of EBL setup leads to the deformation of the proposed structure as illustrated in Fig. 4(a). Therefore, it is necessary to model the metasurface device using simulation techniques to obtain optimized values for the EBL setup to realize high-resolution patterns and ultimately reduce the pattern time. The backscattering of electrons causes the deposition of energy at the different field spots from the actual energy spot area of the exposed pattern configuration [21,22]. The changes occurring in the exposed pattern configuration due to the irradiation of the resist spots or by dose distribution results in the proximity effect. As a result, the pattern resolution between neighboring structures is limited by particle dispersion or the proximity effect [23].

Under the normal setting of the EBL setup, i.e., the acceleration voltage (20 keV), beam width (20 nm), dose (200 $\mu C/cm^2$), the proposed metasurface design is simulated with a 100 nm PMMA resist layer. The energy distribution of backscattered electron trajectories can deposit

Optical Materials EXPRESS

the unwanted energy in unexposed regions, which can not only alter the design pattern but also forms undesirable deformations of the structure. Figure 1(a) illustrates the backscattered electron movement trajectories with normal settings of EBL. It is worth noting, that backscattering not only occurs from the resist layer but also from the chrome and substrate layer. The backscattering can substantially reach the unexposed regions on the resist layer causing deformity of the fabricated structure. Secondly, when fabricating large area metasurface structures, the pattern time is a crucial factor and depends on the dose exposure, step size, and dose currents. The total pattern time can be calculated by the following expressions [24],

$$T_{total} = T_{exposure} + T_{settling} \tag{1}$$

$$T_{exposure} = N_{pixels} * T_{\sin gle\_pixel} \tag{2}$$

$$T_{\sin gle\_pixel} = \frac{Dose * ss^2}{Current} \tag{3}$$

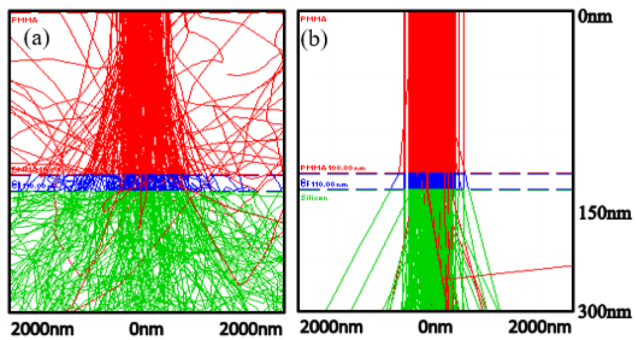

Fig. 1. Simulation of backscattered electron trajectories to control the overexposure resulting from the proximity effect. (a) Simulation results under a normal EBL setup, as the backscattered electron from the resist and substrate layer, expose the undesired areas, which can result in deformation of the metasurface structure. (b) Simulation with our modified method using PEF, since the exposed beam has no backscattering from the resist and substrate layer and only concentrated on the exposed spot area.

The time for patterning depends on the dose rate (keV), step size, beam currents (nA). Optimizing these variables reduces the time required for the patterning on the resist and ultimately increases the throughput. The dose rate also plays a significant role in the reduction of backscattering trajectories when using low voltages as high voltages cause forward scattering. In this study, we have used the point exposure function also known as the point spread function (PSF) to control the proximity effect. To approximate the PSF, Gaussian and exponential functions are used to fit the spatial profile of the electron distribution due to scattering and secondary electron creation. We employ the Gaussian function to describe the backscattered electrons to evaluate the feasibility of our approach for finding the optimized values for EBL settings as given in Table 1. Figure. 1(b) represents our method using PSF; it can be observed that increasing the beam current and decreasing the beam width together with changing the dose rate, controls the backscattering of electrons. The overexposure resulting from the backscattering is alleviated and the pattern is formed on the only exposed area.

The exposure dose for patterning is determined by the electron energy, the backscattered electrons in the resist and substrate, and also by the development environments (i.e., temperature and development time). As a result, we evaluate the development time and temperature in relation to the dose. The exposure simulation yields a comprehensive spatial distribution of the writing beam in the resist. As it is evident, a low exposure dose results in broadening of the beam (See

Optical Materials EXPRESS

Table 1. Parameters used in the EBL patterning process for both methods

Methods	Voltage (keV)	Current (nA)	Beam diameter/ Spot size (nm)	Dose ($\mu C/cm^2$)	Develop Time At T = 22 °C	Write time 2 cm^2
M1	20	0.5	20	200	120 sec	10 hours
M2	50	4.9	10	450	60 sec	3.5 hours

Eq. (4)) producing deformation in the pattern profile [21]. Figure 2(a) represents the dose yield for patterning on the resist under normal conditions (200 $\mu C/cm^2$, 20 keV). The beam width of low energy dose increases and causes overexposure in the undesired area. As a result, the produced developed profile has lower base width and rounded corners at the top surface (shown in Fig. 2(b), thereby altering the entire geometry which can significantly change the resonance behavior of the metasurface. However, to obtain high-resolution developed profiles and to reduce the pattern time, our optimized parametric values from the simulation results outperform the normal condition. The illustration in Fig. 2(c) represents the modified method as the beam width remains the same during the patterning process with less elastic scattering and the beam is only limited to the pattern spots corresponding to the metasurface design. The development profile corresponding to the high dose and controlled proximity effect is presented in Fig. 2(d). The simulation of the developed profile forms a high-resolution pattern with fine corners. When

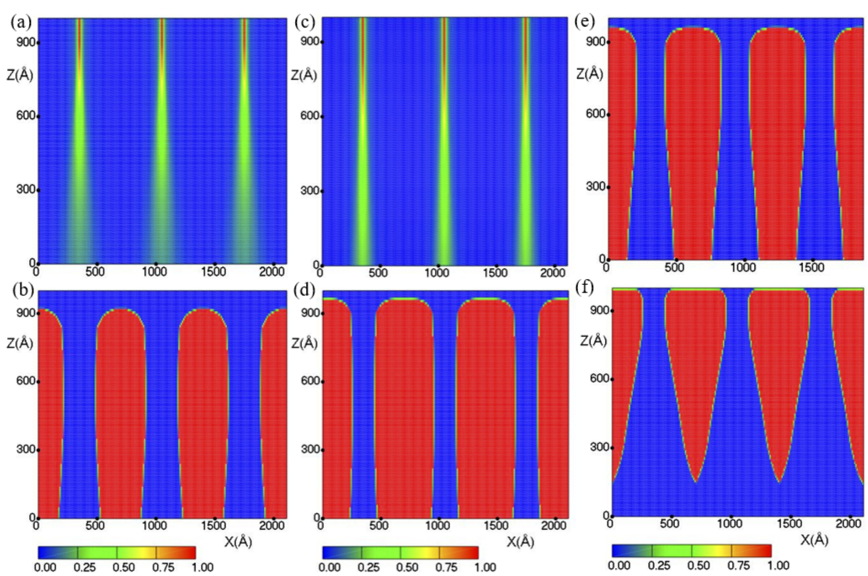

Fig. 2. EBL simulation for dose yield and developed profiles, (a) Beam yield in the resist layer broadens due to elastic scattering when considering low acceleration voltage and low dose currents, (b) The developed profile corresponding to normal settings of EBL with low voltages, as the elastic scattering of electron beam causes overexposure in the resist layer resulting in the deformity of the developed profile, (c) Simulation of the patterning process with controlled proximity effect using high voltage and longer current, these methods also reduce the pattern write time and develop time, (d) Developed profile corresponding to our method, as the profiles in the resist show high resolution along with fine edges, (e) resist the development of our prosed method considering longer time, T = 2 mins, as the profile start the appearance of overdeveloping, (f) T = 3 mins development time results in the degradation of the profile causing pattern collapsing.

Optical Materials EXPRESS

using a high dose the development time decreases, as in this case 60 Sec at 22°C.

$$F(\rho, z) = \frac{3\lambda}{z^3}\left(\frac{-3\lambda\rho}{2z^3}\right)\rho \tag{4}$$

Wherein, λ is the wavelength of the electron transport path in the resist and ρ is the lateral distance of the electron beam axis, as the elastic scattering can be determined from the beam energy and material used for the resist layer. Equation (4) is employed for the uniform distribution of the electron beam to limit the backscattering, resulting in the high spatial distribution of the write beam in the resist layer as shown in Fig. 2(c).

Controlling the fine characteristics that are printable by e-beam depends on the development process. It is crucial to precisely regulate the time and temperature of the resist profile in developing a solution since repeatability is directly correlated with the development time. The phrases underdeveloped and underexposed, or overdeveloped and overexposed, may become a bit ambiguous as a result. The kinetics of the dissolving process plays a significant role in the optimization of EBL needing a thorough understanding of these elements. The issue arises when the resist is overdeveloped (T = 2 mins), the substrate-resist bond weakens and capillarity forces emerge when the solvent is removed as shown in Fig. 2(e). Further increasing the development time to T = 3 mins causes the resist structure to mechanically break, resulting in pattern collapse as illustrated in Fig. 2(f). Particularly for thick resists, adjacent linear features are susceptible to this issue. The relationship between exposure and development can be seen in the fact that shorter exposure with more rapid development can be compared to shorter development with heavier exposure.

3. Fabrication methods for metasurface prototyping

The proximity effect makes it difficult to generate uniform corners in metasurfaces using EBL nanofabrication. The fidelity of the fabricated metasurface array elements to the design has a significant impact on the level of discrepancy between the fabricated and simulated absorption efficiency. In this section, first, the metasurfaces are fabricated under normal conditions using (ELIONIX ELS-7500EX) beam writer for the patterning process depicted in Fig. 4. The pre-cleaned silicon substrate is spin coated (CEE200X) with PMMA (950 K, 2wt % in anisole) resist layer at (2000 rpm, 60 sec) and backed at 150 °C with a metal hotplate for 90 sec to remove residual solvent and raise the adhesion with Si surface. After backing, the PMMA-coated wafer is exposed to an electron beam for pattern writing under normal conditions (200 µC/cm^2, 20 keV) with a beamwidth of 20 nm and step size of 30 nm. The patterned PMMA resist layer is developed in 1:3 (4-methyl-2-pentanone) MBIK: IPA solution for 120 sec and post-backed at 100 °C followed by N_2 blow-drying. The developed patterns are then exposed to thermal evaporation to deposit the pure gold material. The standard liftoff process is performed with an acetone bath to remove the PMMA and unwanted metal from the fabricated metasurface to realize the desired device.

The above method produced distorted corners at the hexagon and cross shape metasurface because of neglecting the proximity effect during the patterning process. When a specific area is exposed to E-beam, the nearby area to the incident E-beam receives undesired irradiation causing a proximity effect. Forward and backward scattered electrons can be used to segregate the exposure of photoresist on a substrate by an E-beam. Secondary electrons can be generated by both scattered electrons, which expose the resist with backscattered electrons having a longer travel distance. Backscattered electrons can reach several tens of micrometers on a Si substrate for high acceleration voltage (>50 keV), causing undesirable photoresist exposure far from the E-beam exposure spot as shown in Fig. 3. Moreover, low dose electron irradiation affects the chemical properties of the PMMA resist resulting in hardening due to long exposure time. The hardened PMMA during the liftoff process increases the possibility of standing unwanted metal on

Optical Materials EXPRESS

the metasurface geometry as shown in Fig. 3(a-d). The small chunks of metal on the metasurface geometry can lead to lower absorption efficiencies. Additionally, the long exposure time for patterning large array elements, the pattern generator can produce an error due to buffer overflow thus restricting the patterning speed. To fabricate the metasurface structures with fine corners and edges the EBL fabrication process is revised with careful considerations to control the proximity effect by using the optimized EBL settings values obtained for PSF through simulations. The measurement of the lithographic PSF by the dot-exposure method, which accounts for all physical phenomena pertinent to EBL exposure, is shown in Fig. 3(e). The comparison between the Monte Carlo Simulation PSF and measured PSF depends on the spot size and secondary electrons (SE) back scattering. These are the absolute limiting factors in EBL for the fabrication of small feature sizes. The results in Fig. 3(e) suggest that PSF becomes lowers as the spot size is decreased, therefore increasing the resolution. The SEs dominate the spatial distribution of deposited energy density in the Monte Carlo simulated PSF. From Fig. 3(e), it can be observed that the simulated PSF is in good agreement with lithographic PSF. For 20 keV exposure, the spread function is higher as the spot size increases which can result in a high proximity effect due to SE scattering. However, Limiting the spot size to 10 nm The PSF can significantly control the SE at 50 keV, thus providing high resolution patterns in the resist. It can be noted, that for the manipulation of PSF for dose distribution, the Gaussian fitting function obtained for each PSF was normalized.

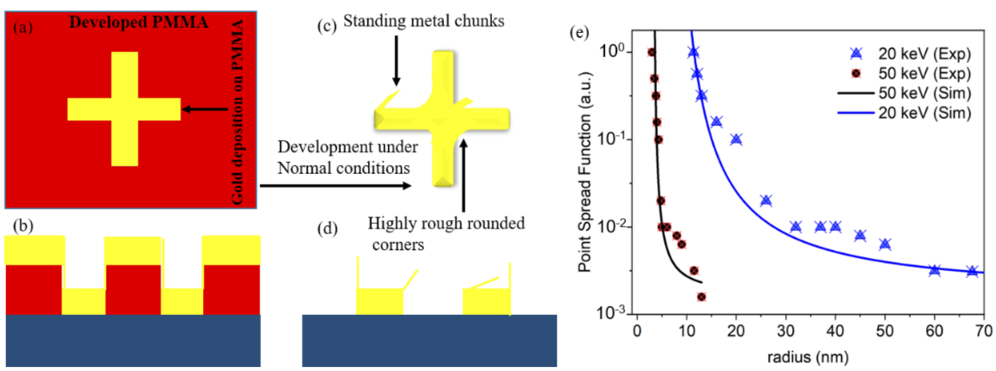

Fig. 3. (a-d) Schematics of the nanofabrication under normal EBL conditions. The hardening of PMMA and over-exposure dose causes standing metal chunks and rough corners, (e) PSF comparison of Monte Carlo simulation versus experimental lithographic PSF, The results are in agreement with optimized simulated results. Employing the optimized parameter in the actual fabrication results in high resolution.

The Si wafer is pre-washed with IPA to remove the environmental impurities. The cleaned wafer substrate is spin coated with 4500 rpm for 60 sec to form a 100 nm PMMA resist layer. Whereas, the time and spin speed can successfully achieve the desired PMMA layer thickness and ultimately reduce the appearance of standing metal chunks on the top surface of the metasurface because the final thickness of the metallic hexagon and cross shape structures are 100 nm respectively. In addition, the thickness of PMMA is measured using a stylus profiler (Dektak XT). The resist-coated wafer is baked at 180°C for 120 sec on a metal hotplate to evaporate the residual solvent. More importantly, for the patterning process, the EBL proximity effect is controlled through proximity effect correction with Gaussian functions to stop the adjacent irradiation SEs in the resist layer.

In the next step, the time and dose for E-beam exposure are critically calculated to reduce the hardening and overexposure on the structure spot to increase the EBL reliability for larger area metasurface fabrication. The patterned PMMA resist is immersed in the developer solution for 60 sec at 22 °C. The longer development time can lead to overdevelopment which can pose

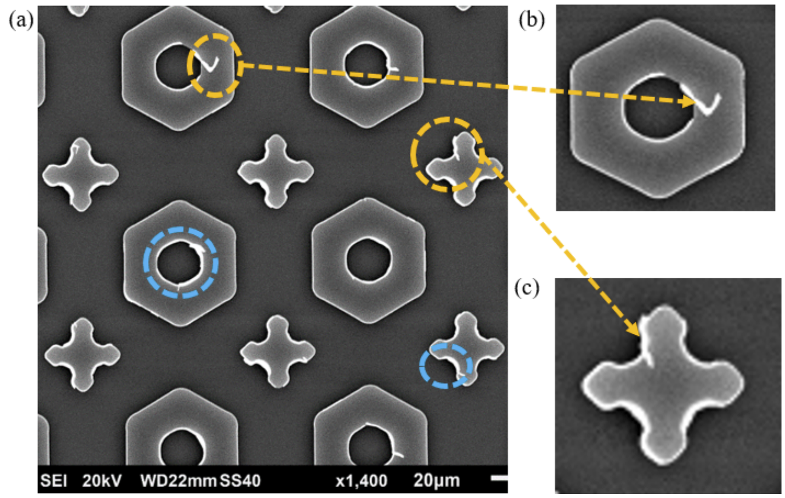

Fig. 4. (a)SEM micrograph of the metasurface fabricated with the first method (M1) in PMMA resist on a silicon substrate with 10 nm chrome layer, exposed to 20 keV with 200 µC/cm^2, develop time is 120 sec in the solution at 22 °C. The resultant image portrays rough corners and rings on the cross-shape absorber. (b) In the zoom micrograph of the hexagon metasurface structure, unwanted metal chunks appeared in the geometry due to the proximity effect and formation of circles at the center as the electron beam has higher dimensions than the feature size, (c) The zoom micrograph of the cross shape fabricated metasurface, the higher deformity is observed in a cross-shape, sharp corners are desired in the geometry but circular shapes appeared at the end of the cross-shape. The altering of the geometry can not only affect the resonance conditions but also lowers the absorption efficiency due to impedance phase matching between the two structures.

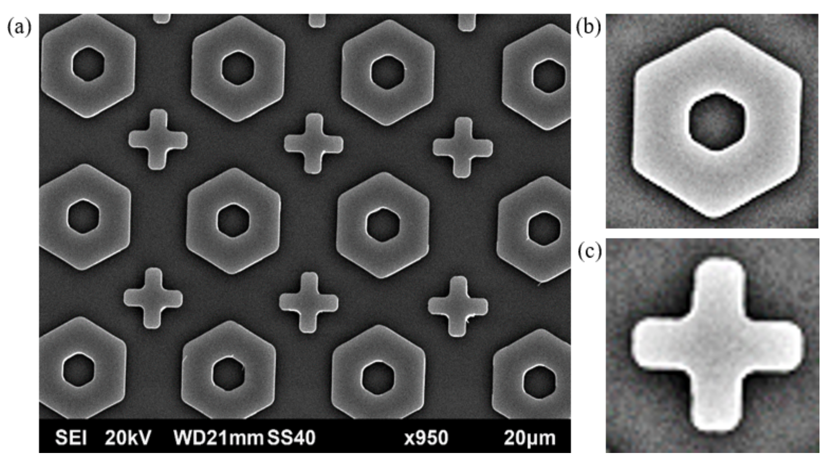

Fig. 5. (a) SEM micrograph of the metasurface fabricated with controlled proximity using PEF resulting in a better quality of fabricated metasurface using (450 µC/cm^2, 50 keV), the development is acquired at 22 °C with a dip for 60 sec in the developer solution. Both the hexagon and cross shape metasurface have sharp edges and fine corners, thus portraying a high resolution of the fabricated structures with enhanced performance, (b, c) Zoom images of the hexagon and cross shape resonator.

Optical Materials EXPRESS

the collapsing of desired geometry. The developed patterns are then subjected to thermal metal evaporation to deposit 10 nm chromium (Cr) and 90 nm of gold (Au) layer at a rate of 1 Å/s having a base pressure of 10^{-5} Torr. The thin layer of Cr material is employed to improve the adhesion of gold material on the substrate surface. In addition, the vertical configuration between the vapor flux and substrate is maintained, so that the angular spread of evaporated vapor flux cannot distort the sharpness of the metasurface structure. The PMMA layer and undesired metal film are removed with a 1-hour acetone bath under ultrasonic treatment during the lift-off procedure. After that, it was rinsed with pure IPA and distilled water for 10 sec before being dried with nitrogen gas. The fabricated metasurface with fine corners is shown in Fig. 5.

4. Structural and optical characterization

Scanning electron microscopy (SEM) at 20 keV was used to examine the surface morphology of the developed metasurfaces featuring plasmonic absorbers. SEM scans in Fig. 4 show the fabricated metasurface under normal conditions. Figure. 5 demonstrate better EBL print consistency (no residue layers) and high-quality patterns at the micrometer scale over large areas. Figure 5 shows a microscopic photo of the uniform pattern of metasurface plasmonic absorbers. The high-resolution SEM photos show that metasurfaces and plasmonic absorbers are distributed evenly across the substrate surface. Infrared spectral measurements are made with a universal attenuated total reflectance and paired with a Fourier transform infrared spectrometer (PerkinElmer) ATR-FTIR with FTIR resolution of (4 cm^{-1}), range (4000 to 650 cm^{-1}), and 20 scans. The manufactured metasurfaces are put on the diamond crystal pointing downwards to touch the gold metasurface layer with the ATR crystal to observe plasmonic absorbance resonance at the LWIR region. A confocal microscope is coupled to an FTIR and a mercury cadmium telluride detector is chilled with liquid nitrogen before readings. An aperture is used to take spectral measurements from a 2000 μm^2 area. A CST simulation tool with FDTD solver was utilized to analyze the absorption resonance of the fabricated metasurface. Periodic boundaries are applied across vertical and horizontal axis with a uniform mesh grid of 0.2 nm, whereas the Palik model [25] is adopted for optical parameters of gold.

5. Results and discussion

The introduction of structural disorders in metasurface fabrication without controlling proximity effect and dose exposure rate can significantly distort absorption resonance. Figure 4 depicts the structural morphology of the metasurface fabricated under normal conditions. It can be observed that the dose exposure (200 $\mu C/cm^2$) and low acceleration voltage (20 keV) leads to the irradiation of E-beam in PMMA layer further resulting in the reduction of fabrication quality and rough curves and highly rounded edges. The main cause of ring development on a cross-shaped metasurface is overexposure of the resist at the irradiation point, followed by carbonization, which implies that the exposed area receives a dose value that is higher than the threshold. Additionally, plasmons field confinement at inner center hexagon slots is weak due to the formation of circular slots shown in Fig. 4(a), whereas hexagon slots are desired to achieve high field plasmonic confinement due to sharp corners. The appearance of the circular metal spot at the cross-shape metasurface (depicted in Fig. 4(c)) is the result of beam broadening due to elastic scattering at lower voltages. The resultant fabricated profile is in agreement with the developed simulation profile as shown in Fig. 2(b), the edges of the metasurface tend to be circular at the ends which can shift the resonance of the metasurface. Another key use of simulation modeling of the resist developed profiles is to supplement experimental research by forecasting basic EBL process trends. It can also be used to predict the process conditions for future refinement. Similarly, it can be observed from Fig. 4(b-c) that the appearance of the standing metal depends on overexposure, beam width, and step size. The larger beam width and step size produce high backscattering of moving electrons, which causes the resist hardening in desired spots. In Fig. 4(b), the geometry of the inner hexagons appeared as symmetric circles because the broader beam width lacks the functionality of patterning small feature sizes.

In our method, consistent dosage of 450 μC/cm^2 is applied to a 1000 μm ×1000 μm field writing area. Selecting a larger field area, the pattern can be replicated with ten times lesser write fields. As an outcome, the sample stage movement time and subsequent stage settling time will be reduced by a factor of 100. It should be noted that the area corresponds to the spot area exposed by the beam, not the total pattern area, as in this case, the total pattern area is 1 cm^2. The convolution of the PSF and the disc in the layout (area step size) determines the total exposure in any given region. A series of procedures are required to experimentally determine the PSF and are reliant on the resist contrast and processing conditions. To achieve uniform exposure on the resist by the e-beam over the designed area, EBL proximity effect correction (PEC) is also applied with different exposure dosages and pattern proximity correction to adjust the local structural detail of the design and to ensure that the fabricated metasurface reliably follows the modeled structure. Because of its considerable effect on the electron penetration depth and the number of inelastic collisions happening in the resist, the electron beam energy plays a critical role in the fabrication process. When the electron energy increases (>50 keV), the penetration depth increases, resulting in a narrow primary electron energy density distribution in the resist. At increasing voltages, the number of polymer chain scissions per electron falls. Therefore, during fabrication to control the proximity effect, the acceleration voltage is kept at 50 keV with an exposure dose of 450 μC/cm^2. We note when the pattern is exposed to a high dose, the developed profiles retain their shape according to the designed geometry. The SEM images in Fig. 5(a-c) illustrate the fabrication of a large area metasurface with the above-controlled conditions resulting in fine corners and edges. The high current with a stable dose allows for manufacturing over relatively wide regions in a short amount of time.

The optical characterization of the fabricated metasurfaces is experimentally demonstrated by utilizing FTIR spectroscopy. Figure. 6(a) depicts the absorption spectra of both fabricated metasurfaces and the FDTD simulation model. The black dotted line represents the FDTD absorption resonance of the metasurface, which is in close agreement with the result of the prototype fabricated according to our method. The proposed device has a plasmonic resonance at 8μm LWIR region with an absorption bandwidth of 2μm. The resultant high absorption at 8 μm is due to plasmons field enhancement at sharp corners and efficient interaction of plasmonic fields between the cross shape and hexagon shape metasurface. It can be noted, to achieve higher absorption both structures should be impedance matched. The mismatching can result in lower coupling of a plasmonic field on the metasurface acquiring low efficiency and sensitivity. The red line in Fig. 6(a) indicates the absorption resonance with rough edges fabricated with M1. The roughness of the structure decreases the plasmonic interaction with incident light and thereby reduces the field confinement. The low field confinement acquires low absorption 55%. The shift in resonance is caused by the appearance of highly rounded corners with rough geometry. The rounded corners increase the surface area of the resonator, which shifts the resonance absorption towards longer wavelengths. Whereas, the sharp-cornered metasurface achieves almost 90% absorption at 8 μm resonance.

This resonance should be attributed to localized surface plasmon resonance (LSPR) i.e., efficient coupling of adjacent array elements. When sharp edges metasurfaces are exposed to incident light of resonance wavelength, the plasmonic resonance concentrates at corners and significantly increases the field energy density. This effect is normally dependent on the sharpness of the metasurface. The metasurface prototype in Fig. 6(b), (c) has a strong spatial concentration of electric field at the center of hexagon slots. The LSPR exceptionally strong and confined electromagnetic fields may be used to create a highly sensitive probe for detecting minute changes in the dielectric environment. The refractive index of the immediate surroundings around a metal metasurface structure increases bimolecular binding events move closer to the surface.

Optical Materials EXPRESS

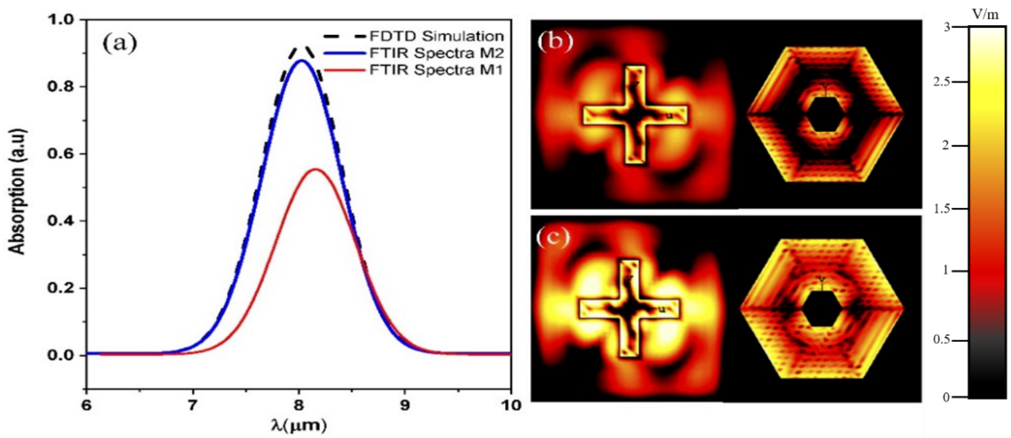

Fig. 6. (a) FTIR absorption spectra of fabricated metasurface devices with sharp corners and rough surface edges and their comparison with simulation. (b), (c) The IR image of plasmonic field confinement and their propagation on the sharp edges and corners.

Thus, bimolecular interactions at the metasurface structure surface immediately cause local refractive index changes, which can be tracked using the LSPR peak absorption wavelength shift. Furthermore, our proposed fabrication method is compared with the literature studies in Table 2.

Table 2. Comparison of our work with literature

Refs	Size	Absorption %	Structural Quality	Fabrication Method
[26]	450 × 450 µm	88	Extremely rough and distorted in shape	EBL
[27]	2 × 3 cm	88.27	Appearance of highly rounded corners with lower resolution	Maskless direct laser lithography
[28]	1.5×1.5 cm^2	25	Circular shape deformation to oval shape with irregular edges	EBL
[29]	100 mm^2	-	Lower resolution with nonuniform shapes	EBL
This work	2×2 cm^2	90	High resolution with uniformity in arrays shape and edges	Modified EBL

6. Conclusion

In conclusion, an experimental demonstration of metasurface nanofabrication with a controlled proximity effect is presented. The controlled conditions in EBL, specifically PEC and PSF solve the long-standing problem of Nano lithographic production of the sharp metasurface, enabling high production and repeatability in larger areas. The key advantage of the proposed method i.e., low dwell time for exposure, more efficient delivery of energy to ultrathin resist and lower probability of sample damage. Using a high exposure dose with longer currents results in less patterning time over a larger area. When compared to traditional EBL, arrays of metasurface nanostructures may be easily scaled to huge regions with a three-fold reduction in exposure time. The FTIR spectra revels the higher absorption resonance at 8 µm with 90% absorption, thus approving the plasmonic field enhancement with sharp edges and corners. Rough corners can ultimately reduce the plasmon enhancement and result in lower absorption sensitivity Nonetheless, this research has taken a promising step toward high-quality plasmonic metasurfaces for quantum optics, biosensing, and optical imaging applications.

Optical Materials EXPRESS

Funding. Abu Dhabi Research Excellence Award (AAREI19-245).

Acknowledgments. This work is a part of collaboration between College of Engineering, AL Ain University and Faculty of Electrical Engineering, Universiti Teknologi PETRONAS. We also like to acknowledge the efforts and contributions made towards this research topic by Durham university, UK.

Disclosures. The authors declare no conflict of interests.

Data availability. Data underlying the results presented in this paper are not publicly available at this time but may be obtained from the authors upon reasonable request.

References

1. M. S. Bin-Alam, O. Reshef, Y. Mamchur, M. Z. Alam, G. Carlow, J. Upham, B. T. Sullivan, J. M. Ménard, M. J. Huttunen, R. W. Boyd, and K. Dolgaleva, "Ultra-high-Q resonances in plasmonic metasurfaces," Nat. Commun. **12**(1), 1–8 (2021).
2. Q. Wang, B. Gao, M. Raglione, H. Wang, B. Li, F. Toor, M. A. Arnold, and H. Ding, "Design, Fabrication, and Modulation of THz Bandpass Metamaterials," Laser Photonics Rev. **13**(11), 1900071 (2019).
3. A. Scidà, S. Haque, E. Treossi, A. Robinson, S. Smerzi, S. Ravesi, S. Borini, and V. Palermo, "Application of graphene-based flexible antennas in consumer electronic devices," Mater. Today **21**(3), 223–230 (2018).
4. H. Hu, X. Yang, F. Zhai, D. Hu, R. Liu, K. Liu, Z. Sun, and Q. Dai, "Far-field nanoscale infrared spectroscopy of vibrational fingerprints of molecules with graphene plasmons," Nat. Commun. **7**(1), 12334 (2016).
5. M. H. Mubarak, O. Sidek, M. R. Abdel-Rahman, M. T. Mustaffa, A. S. Mustapa Kamal, and S. M. Mukras, "Nano-antenna coupled infrared detector design," Sensors **18**(11), 3714 (2018).
6. S. Aksu, M. Huang, A. Artar, A. A. Yanik, S. Selvarasah, M. R. Dokmeci, and H. Altug, "Flexible plasmonics on unconventional and nonplanar substrates," Adv. Mater. **23**(38), 4422–4430 (2011).
7. S. Aksu, A. A. Yanik, R. Adato, A. Artar, M. Huang, and H. Altug, "High-throughput nanofabrication of infrared plasmonic nanoantenna arrays for vibrational nanospectroscopy," Nano Lett. **10**(7), 2511–2518 (2010).
8. I. Epstein, D. Alcaraz, Z. Huang, V. V. Pusapati, J. P. Hugonin, A. Kumar, X. M. Deputy, T. Khodkov, T. G. Rappoport, J. Y. Hong, N. M. R. Peres, J. Kong, D. R. Smith, and F. H. L. Koppens, "Far-field excitation of single graphene plasmon cavities with ultracompressed mode volumes," Science **368**(6496), 1219–1223 (2020).
9. M. Zhang, V. Pacheco-Peña, Y. Yu, W. Chen, N. J. Greybush, A. Stein, N. Engheta, C. B. Murray, and C. R. Kagan, "Nanoimprinted chiral plasmonic substrates with three-dimensional nanostructures," Nano Lett. **18**(11), 7389–7394 (2018).
10. C. Williams, G. S. D. Gordon, T. D. Wilkinson, and S. E. Bohndiek, "Grayscale-to-color: scalable fabrication of custom multispectral filter arrays," ACS Photonics **6**(12), 3132–3141 (2019).
11. S. Fasold, S. Linß, T. Kawde, M. Falkner, M. Decker, T. Pertsch, and I. Staude, "Disorder-enabled pure chirality in bilayer plasmonic metasurfaces," ACS Photonics **5**(5), 1773–1778 (2018).
12. S. Daqiqeh Rezaei, J. Ho, T. Wang, J. K. W. Yang, and S. Ramakrishna, "Direct color printing with an electron beam," Nano Lett. **20**(6), 4422–4429 (2020).
13. R. P. Jenkins, S. D. Campbell, and D. H. Werner, "Establishing exhaustive metasurface robustness against fabrication uncertainties through deep learning," Nanophotonics **10**(18), 4497–4509 (2021).
14. Y. Fan, B. Cluzel, M. Petit, X. Le Roux, A. Lupu, and A. De Lustrac, "2D waveguided Bessel beam generated using integrated metasurface-based plasmonic axicon," ACS Appl. Mater. Interfaces **12**(18), 21114–21119 (2020).
15. F. Sterl, E. Herkert, S. Both, T. Weiss, and H. Giessen, "Shaping the color and angular appearance of plasmonic metasurfaces with tailored disorder," ACS Nano **15**(6), 10318–10327 (2021).
16. B. Malekian, K. Xiong, E. S. H. Kang, J. Andersson, G. Emilsson, M. Rommel, T. Sannomiya, M. P. Jonsson, and A. Dahlin, "Optical properties of plasmonic nanopore arrays prepared by electron beam and colloidal lithography," Nanoscale Adv. **1**(11), 4282–4289 (2019).
17. A. Samardak, M. Anisimova, A. Samardak, and A. Ognev, "Fabrication of high-resolution nanostructures of complex geometry by the single-spot nanolithography method," Beilstein J. Nanotechnol. **6**(1), 976–986 (2015).
18. Y. Liang, H. Lin, K. Koshelev, F. Zhang, Y. Yang, J. Wu, Y. Kivshar, and B. Jia, "Full-Stokes polarization perfect absorption with diatomic metasurfaces," Nano Lett. **21**(2), 1090–1095 (2021).
19. B. R. Lu, J. Deng, Q. Li, S. Zhang, J. Zhou, L. Zhou, and Y. Chen, "Reconstructing a plasmonic metasurface for a broadband high-efficiency optical vortex in the visible frequency," Nanoscale **10**(26), 12378–12385 (2018).
20. I. Kim, J. Mun, K. M. Baek, M. Kim, C. Hao, C. W. Qiu, Y. S. Jung, and J. Rho, "Cascade domino lithography for extreme photon squeezing," Mater. Today **39**(October), 89–97 (2020).
21. M. Astrand, T. Frisk, H. Ohlin, and U. Vogt, "Understanding dose correction for high-resolution 50 keV electron-beam lithography on thick resist layers," Micro Nano Eng. **16**, 100141 (2022).
22. M. M. Rahman, A. Raza, H. Younes, A. AlGhaferi, M. Chiesa, and J. Lu, "Hybrid graphene metasurface for near-infrared absorbers," Opt. Express **27**(18), 24866 (2019).
23. A. E. Rogozhin and F. A. Sidorov, "E-beam lithography simulation techniques," Russ. Microelectron. **49**(2), 108–122 (2020).
24. M. Stepanova, T. Fito, Z. Szabó, K. Alti, A. P. Adeyenuwo, K. Koshelev, M. Aktary, and S. K. Dew, "Simulation of electron beam lithography of nanostructures," J. Vac. Sci. Technol., B: Nanotechnol. Microelectron.: Mater., Process., Meas., Phenom. **28**(6), C6C48–C6C57 (2010).

Optical Materials EXPRESS

25. P. B. Johnson and R. W. Christy, "Optical constant of the nobel metals," Phys. Rev. B **6**(12), 4370–4379 (1972).
26. A. K. Azad, W. J. M. Kort-Kamp, M. Sykora, N. R. Weisse-Bernstein, T. S. Luk, A. J. Taylor, D. A. R. Dalvit, and H. T. Chen, "Metasurface broadband solar absorber," Sci. Rep. **6**, 20347 (2016).
27. C. Chen, Y. Liu, Z. Jiang, C. Shen, Y. Zhang, F. Zhong, L. Chen, S. Zhu, and H. Liu, "Large-area long-wave infrared broadband all-dielectric metasurface absorber based on markless laser direct writing lithography," Opt. Express **30**(8), 13391 (2022).
28. B. Du, Z. Wu, J. Xia, J. Wu, G. Tong, and H. Zhang, "Large-area all-dielectric metasurface fabricated by an anodized aluminum oxide template," Opt. Express **29**(7), 10465 (2021).
29. H. Hemmati, P. Bootpakdeetam, K. J. Lee, and R. Magnusson, "Rapid large-scale fabrication of multipart unit cell metasurfaces," Opt. Express **28**(13), 19304 (2020).